

Universal time-temperature scaling of conductivities in random site energy and associated random barrier model

Sven Lohmann,^{1,*} Quinn Emilia Fischer,^{1,†} Justus Leiber,^{1,‡} and Philipp Maass^{1,§}

¹*Universität Osnabrück, Institut für Physik, Barbarastrasse 7, D-49076 Osnabrück, Germany*

(Dated: January 13, 2026)

Universal time-temperature scaling of conductivity spectra in disordered solids has been explained by thermally activated hopping of noninteracting particles over random energy barriers. An open problem is whether the random barrier model accounts for site energy disorder in real materials. Through mapping many-particle hopping in a disordered site energy landscape to that of independent particles in a barrier landscape, we show that time-temperature scaling is correctly described by the associated barrier model in the low temperature limit. However, the site energy model displays good scaling behavior at substantially higher temperatures than the barrier model, in agreement with experimental observations. Extending the mapping to different types of mobile charge carriers allows us to understand why time-temperature superposition can be absent in mixed alkali glasses.

I. INTRODUCTION

Conductivities of disordered solid materials exhibits universal scaling properties at frequencies below 100 GHz [1, 2]. Spectra $\sigma(\omega) = \sigma'(\omega) + i\sigma''(\omega)$ at different temperatures T fall onto a single master curve when $\sigma(\omega, T)$ is normalized to the dc conductivity σ_{dc} and the frequency scaled with $\sigma_{dc}/\Delta\epsilon$:

$$\frac{\sigma(\omega, T)}{\sigma_{dc}} = F\left(\frac{\Delta\epsilon\omega}{\sigma_{dc}}\right). \quad (1)$$

Here, $\Delta\epsilon = \lim_{\omega \rightarrow 0} [\sigma''(\omega, T)/\omega]$ is the difference between the dielectric permittivities at low and high frequencies. Frequency-temperature scaling, also referred to as time-temperature superposition principle, is observed for electron conduction in amorphous semiconductors [1, 3–6], polymers [7–9], organic-inorganic hybrid compounds [10], and polymer-carbon nanotube thin films [11], for polaron-mediated electron transport [12–14], as well as for ion conduction in polymer electrolytes [15–18] and glasses [19–47].

The dc conductivity is generally thermally activated, $T\sigma_{dc} = A \exp(-E_{dc}/k_B T)$, where A is the pre-exponential factor and E_{dc} the activation energy. In disordered electron conductors, variable range hopping can be relevant, leading to Mott’s law, $\ln \sigma_{dc} \sim -1/T^{1/4}$. The dielectric strength $\Delta\epsilon$ depends weakly on temperature, often according to a Curie law, $\Delta\epsilon \propto 1/T$. Scaling functions $F(\cdot)$ are very similar for different materials, albeit not exactly the same.

A scaling behavior according to Eq. (1), with $\Delta\epsilon$ replaced by a related factor, was predicted theoretically and verified for materials [1] based on the extended pair approximation [48] for hopping transport and later interpreted by refined theoretical approaches [49–51]. Dyre

and Schröder showed that Eq. (1) can be accounted for by the Random Barrier Model (RBM) [52–57], where independent particles perform thermally activated hops over random, uncorrelated energy barriers of a lattice. For dimensions larger than two at low temperatures, corresponding to an “extreme disorder limit”, they derived the relation [58]

$$\ln \tilde{\sigma} = \frac{i\tilde{\omega}}{\tilde{\sigma}} \left(1 + 2.66 \frac{i\tilde{\omega}}{\tilde{\sigma}}\right)^{-1/3} \quad (2)$$

between the normalized conductivity $\tilde{\sigma} = \sigma/\sigma_{dc}$ and scaled frequency $\tilde{\omega} = \epsilon_0 \Delta\epsilon \omega / \sigma_{dc}$ based on an improved variant of the diffusion-cluster-approximation [59]. Equation (2) gives the scaling function $F(\cdot)$ in the RBM very accurately and provides a good approximation also for scaling functions of real materials.

In amorphous solids, disorder is present also in energies of sites, which represent potential wells where charge carriers reside for a long time before passing a barrier in a rare thermally activated transition. This site energy disorder was shown to be important, in particular, for understanding compositional effects in ion conducting glasses, as, e.g., the mixed alkali [60–78] and mixed glass former effect [79–93]. The site energy disorder requires to take into account particle interactions, because independent particles would accumulate at the sites with lowest energy at low T . In view of this, one may wonder why the conductivity scaling (1) can be successfully described by the RBM, where sites have equal energy and a hopping motion of independent particles is considered.

In this article we tackle this question by studying the Random Site Energy Model (RSEM) with site-exclusion interaction, i.e. each lattice site can be occupied by at most one particle. This model can be viewed a minimal model for thermally activated particle transport in disordered solids with site energy disorder. We are not considering variable-range hopping in this study, which would be important for electron tunneling. With respect to time-temperature scaling features, the RSEM was studied before in two dimensions based on a linearized version of the master equation [94], and in three dimensions

* slohmann@uni-osnabrueck.de

† qfischer@uni-osnabrueck.de

‡ jleiber@uni-osnabrueck.de

§ maass@uni-osnabrueck.de

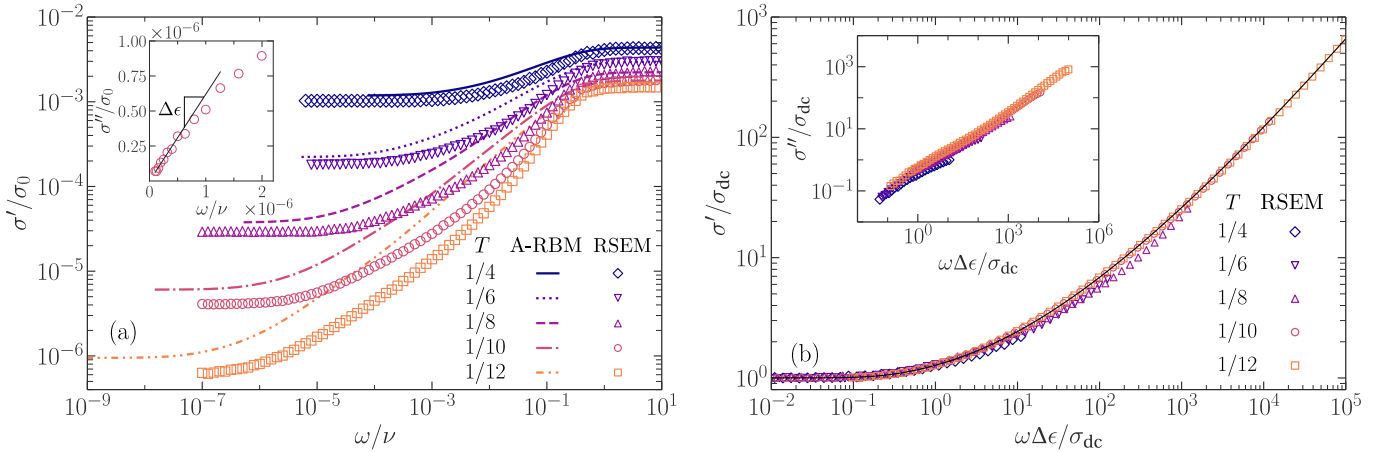


FIG. 1. (a) Real parts $\sigma'(\omega, T)$ of conductivity spectra for five different temperatures. Symbols refer to the RSEM and lines to the A-RBM. The inset shows the imaginary part $\sigma''(\omega, T)$ for $T = 1/10$ on linear axes scales, where $\Delta\epsilon(T)$ is extracted from the low-frequency behavior $\sigma''(\omega, T) \sim \Delta\epsilon \omega$. (b) Scaled spectra for frequencies one order of magnitude below the attempt frequency, $\omega \leq \nu/10$. The inset shows the correspondingly scaled imaginary parts of the conductivity. Data for the RSEM and A-RBM were obtained by averaging over 100 realizations of site energies. The solid line represents the master curve given by Eq. (2).

by percolation theory [50, 51] and simulations of time-dependent diffusion coefficients [95].

The RSEM is fundamentally different from the RBM because it is a many-particle model with site exclusion interaction. This becomes immediately evident when considering the variation of activation energies upon changing the concentration n of mobile charge carriers in a fixed energy landscape: in the RBM with noninteracting particles, ion mobilities are independent of n . The conductivity activation energy does not depend on ion concentration and the conductivity is proportional to it. In contrast, the activation energy in the RSEM has a strong nonlinear dependence on ion concentration.

This is just one fundamental difference between the RSEM and RBM. Another one concerns the preferential occupation of low energy sites in the RSEM below the Fermi energy. Even when comparing hopping dynamics of a single particle in a potential landscape with random traps and saddle points on equal level, the two models are very different, because high energy barriers are mainly avoided in the diffusive motion of a single particle, while deep traps are not. In fact, the conductivity is independent of frequency in random trap model of noninteracting particles [96].

Despite these fundamental differences, we here relate particle hopping in the RSEM to that of an associated random barrier model (A-RBM) and demonstrate that time-temperature scaling of conductivities in the A-RBM agrees with that in the RSEM. However, scaling in the RSEM sets in at scaled temperatures $k_B T/E_{dc}$ higher than in the A-RBM, in agreement with experimental observations. This suggests that site energy variations and many-particle dynamics are important also to understand time-temperature superposition in real materials.

II. SCALING OF CONDUCTIVITY SPECTRA IN THE RANDOM SITE ENERGY MODEL

For our analysis of the RSEM, we choose a simple cubic lattice with lattice constant a and assign to each site i a random site energy E_i drawn from a Gaussian distribution with zero mean and standard deviation Δ_E . The particle concentration is $n = 0.9 a^{-3}$, corresponding to a typical vacancy concentration in ion conducting glasses [97–99]. In the absence of an electric field, particles jump from occupied sites i to vacant nearest neighbor sites j with the Metropolis hopping rates

$$w_{ij} = \nu \min(1, \exp[-(E_j - E_i)/k_B T]) \\ = w(\beta(E_i - E_j)), \quad (3)$$

where ν is an attempt frequency and $\beta = 1/k_B T$. We perform kinetic Monte Carlo (KMC) simulations and determine $\sigma(\omega, T)$ by applying the method described in Ref. [100]. Details are given in Appendix A.

As units of length, time and energy we use a , ν^{-1} , and Δ_E respectively, and as unit of conductivity $\sigma_0 = nq^2 \nu a^2 / \Delta_E$, where q is the particle charge.

Figure 1(a) shows $\sigma'(\omega, T)$ for the RSEM (symbols) at five temperatures T . These real parts of the spectra monotonically increase with ω from the dc-value σ_{dc} to the high-frequency plateau σ_∞ , where the dispersion strength $\sigma_\infty/\sigma_{dc}$ is the stronger the lower the temperature. From the linear increase $\sigma''(\omega, T) \sim \Delta\epsilon \omega$ for $\omega \rightarrow 0$, we extract the dielectric strengths $\Delta\epsilon(T)$, see the inset of Fig. 1(a) for an example.

Figure 1(b) shows that a scaling according to Eq. (1) yields a data collapse onto a common master curve for frequencies $\omega \leq \nu/10$ one order of magnitude smaller than the attempt frequency ν . As ν is of the order of

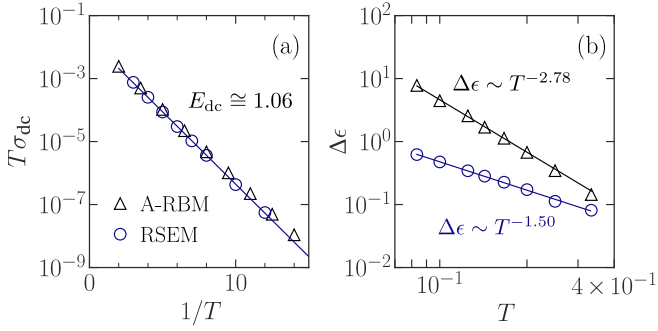


FIG. 2. (a) Arrhenius plots of dc-conductivities in the RSEM and A-RBM. A least squares fit to the data (solid line) yields an activation energy $E_{dc} \cong 1.06$. (b) Dielectric strength $\Delta\epsilon$ as a function of temperature for the two models. Least squares fits to power laws (solid lines, fit for $T \leq 1/6$ for the A-RBM) yield $\Delta\epsilon \sim T^{-1.50}$ (RSEM) and $\Delta\epsilon \sim T^{-2.78}$ (A-RBM).

phonon frequencies $\nu \simeq 10^{11-13} \text{ s}^{-1}$, this regime corresponds to that below ~ 100 GHz, where scaling of conductivity spectra is observed [101]. We further focus on this frequency range relevant for experiments.

The temperature dependence of the scaling parameters σ_{dc} and $\Delta\epsilon$ of the RSEM (circles) is displayed in Fig. 2. From a least squares fit to σ_{dc} in the Arrhenius plot of Fig. 2(a), we obtain an activation energy $E_{dc} \cong 1.06$. Evaluating $T\sigma_{dc}(T) \exp(E_{dc}/k_B T)$ for different T , we find the preexponential $A \cong 0.018$ to be independent of T . In the simulated temperature range, the dielectric strength in the double-logarithmic plot of Fig. 2(b) can be fitted by a power law $\Delta\epsilon \sim T^{-1.50}$.

III. MAPPING OF RANDOM SITE ENERGY ONTO RANDOM BARRIER MODEL

For relating the RSEM to a barrier model, we use the theory of Ambegaokar, Halperin and Langer (AHL theory) [102]. According to this theory, dc-transport in the RSEM is described by a mapping onto a random resistor network [103] with symmetric link conductances.

$$g_{ij} = \beta q^2 w_{ij} \langle n_i \rangle_{\text{eq}} (1 - \langle n_j \rangle_{\text{eq}}) = g_{ji}. \quad (4)$$

Here, $\langle n_i \rangle_{\text{eq}}$ are the mean occupation numbers in equilibrium,

$$\langle n_i \rangle_{\text{eq}} = f(\beta(E_i - \mu)), \quad (5)$$

with $f(x) = 1/(e^x + 1)$ the Fermi function and μ the chemical potential.

We extend the mapping to dispersive ac-transport by considering independent particles to hop between nearest neighbor sites i, j with rates $\nu \exp(-\beta U_{ij})$, where the energy barriers $U_{ij} = U_{ji}$ are obtained by identifying the rate $w_{ij} \langle n_i \rangle_{\text{eq}} (1 - \langle n_j \rangle_{\text{eq}})$ in Eq. (4) with the hopping

rate $\nu \exp(-\beta U_{ij})$:

$$U_{ij} = U(E_i, E_j) = -\frac{1}{\beta} \ln \min(1, \exp[-\beta(E_j - E_i)]) - \frac{1}{\beta} \ln(f(\beta(E_i - \mu)) [1 - f(\beta(E_j - \mu))]). \quad (6)$$

These barriers define the barrier landscape of the A-RBM. They depend on temperature, and on the particle concentration n via the chemical potential μ .

By setting the particle concentration equal to one in the A-RBM, we ensure that σ_{∞} is equal to that in the RSEM. This is shown in Appendix B.

A. Barrier distribution and correlations

Distributions of the barriers in the A-RBM are well described by Gaussians truncated at $U = 0$. This is demonstrated for $T = 1/4$ and $T = 1/12$ in Fig. 3. The distribution at the lower $T = 1/12$ is representative for the $T \rightarrow 0$ limit, where $U_{ij} = (|E_i - E_j| + |E_i - E_F| + |E_j - E_F|)/2$ and $E_F = \mu(T \rightarrow 0) = \sqrt{2\Delta_E} \text{erf}^{-1}(2n-1) \cong 1.28$ is the Fermi energy. That $T = 1/12$ corresponds to the $T \rightarrow 0$ limit can be understood by noting that for a non-truncated Gaussian $\mu \sim E_F [1 + (\pi k_B T / \sqrt{6\Delta_E})^2]$ for $T \rightarrow 0$, yielding a crossover temperature $T_x = \sqrt{6\Delta_E} / \pi k_B \cong 0.78$. Hence, $T \ll T_x$ for $T = 1/12 \cong 0.083$.

The U_{ij} of neighboring links are correlated even for spatially uncorrelated site energies E_i . The autocorrelation $C_U = \langle U_{ij} U_{kl} \rangle - \langle U_{ij} \rangle^2$ for neighboring links (ij)

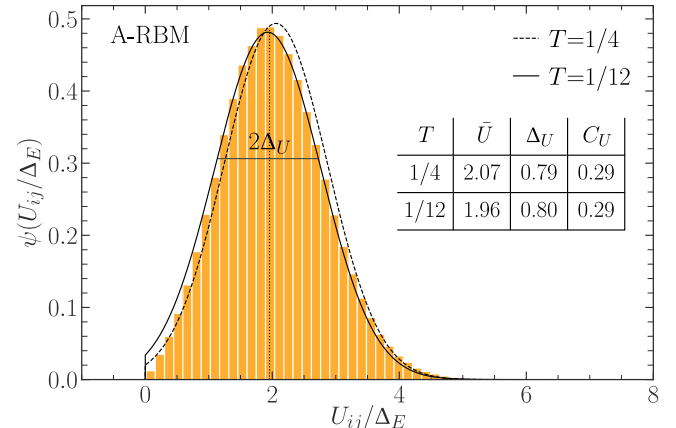


FIG. 3. Histogram of energy barriers U_{ij} [Eq. (6)] in the A-RBM for $T = 1/12$. It can be described by a truncated Gaussian (solid line) with mean \bar{U} and standard deviation Δ_U of the barrier distribution. Since $T = 1/12$ is in the low-temperature regime (see text), the truncated Gaussian represents also the barrier distribution in the limit $T \rightarrow 0$. At higher T , slight changes occur, as demonstrated by the truncated Gaussian describing the histogram at $T = 1/4$. The table gives \bar{U} , Δ_U , and the correlation $C_U = \langle U_{ij} U_{kl} \rangle - \langle U_{ij} \rangle^2$ between barriers at neighboring links (ij) and (kl) .

and (kl) is given in the table in Fig. 3, together with the variance $\Delta_U^2 = \langle U_{ij}^2 \rangle - \langle U_{ij} \rangle^2$ of the barrier distributions.

IV. COMPARISON OF CONDUCTIVITY SCALING IN A-RBM AND RSEM

For calculating $\sigma(\omega, T)$ of the A-RBM we apply the velocity autocorrelation (VAC) method [104]. The determining equations are given in Appendix C. Real parts $\sigma'(\omega, T)$ are compared with the RSEM in Fig. 1(a), and data for σ_{dc} and $\Delta\epsilon(T)$ in Figs. 2(a) and (b).

In the temperature regime $1/12 \leq T \leq 1/4$ of the data in Fig. 1, the dc-conductivity of the A-RBM (triangles) agrees well with that of the RSEM (circles), see Fig. 2(a). This is surprising because nearest-neighbor correlations between occupation numbers in the state of constant current are factorized in the AHL theory. This approximation, however, becomes worse at lower temperatures, causing σ_{dc} of the A-RBM to differ from that of the RSEM. The increasing difference with lower T is also visible when comparing the low-frequency data in Fig. 1(a).

The VAC method allows one to calculate conductivities or the A-RBM with high numerical accuracy at very low temperatures $T < 10^{-2}$. Arrhenius plots of dc-conductivities are shown in Fig. 4 for β up to 50 and a least squares fit in the range $16 \leq \beta \leq 50$ yields the activation energy $E_{dc} \cong 0.97$ (orange line). This value is in agreement with a percolation analysis based on the zero-temperature limit of the barriers in Eq. (6),

$$U_{ij}(T \rightarrow 0) = \frac{1}{2} (|\varepsilon_i - \varepsilon_j| + |\varepsilon_i - \varepsilon_F| + |\varepsilon_j - \varepsilon_F|). \quad (7)$$

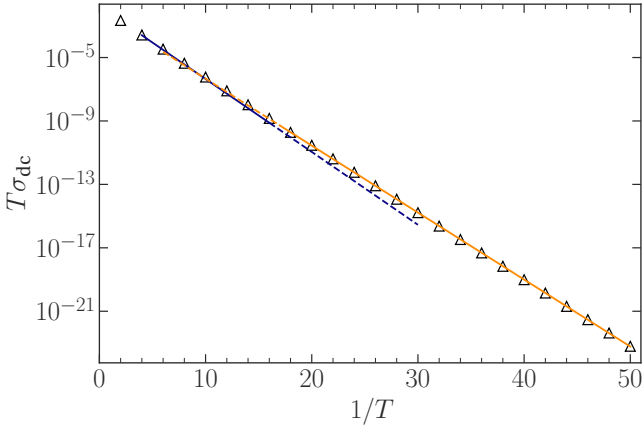


FIG. 4. Arrhenius plot of dc-conductivities of the A-RBM calculated from Eq. (C1). The activation energy $E_{dc} \cong 0.97$ obtained from a least squares fit in the range $16 \leq \beta \leq 50$ (orange line) is in agreement with a percolation analysis based on the barriers in the limit $T \rightarrow 0$ [Eqs. (7),(8)]. A least squares fit in the range $4 \leq \beta \leq 15$ (blue line) yields the apparent activation energy $E_{dc} \cong 1.06$ that agrees with the activation energy of the RSEM in Fig. 2a.

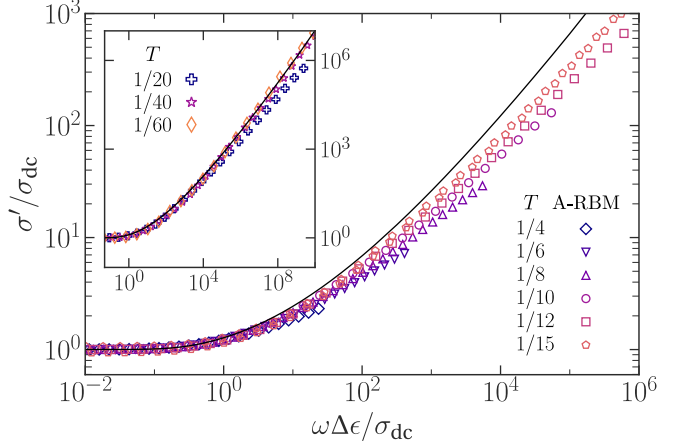


FIG. 5. Scaled real parts of conductivity spectra in the A-RBM for temperatures $T \geq 1/15$, yielding no data collapse onto the master curve given by Eq. (2) (solid line). The scaled data in the inset show that scaling behavior sets in at lower temperatures $T \lesssim 1/40$.

According to this analysis,

$$E_{dc} = \min \left\{ U_x \mid \begin{array}{l} \text{links } (ij) \text{ with } U_{ij}(T \rightarrow 0) < U_x \\ \text{form a percolating path} \end{array} \right\}. \quad (8)$$

We have determined the minimum by applying the Hoshen-Kopelman algorithm [105] to large systems of 200^3 sites, yielding a sharp percolation threshold at $\min\{U_x \mid \dots\} = E_{dc} \cong 0.97$.

This activation energy of the A-RBM is lower than $E_{dc} \cong 1.06$ in Fig. 2(a). Accordingly, E_{dc} in Fig. 2(a) is an apparent one for the A-RBM. For the RSEM by contrast, our analysis suggests that $E_{dc} \cong 1.06$ is the true activation energy for $T \rightarrow 0$.

The dielectric strength of the A-RBM has a temperature dependence different from the RSEM. Data are presented in Fig. 2(b) and can be fitted by a power law behavior $\Delta\epsilon \sim T^{-2.78}$ in the considered temperature range.

Let us now consider the scaling behavior in the A-RBM. Due to the different temperature dependencies of $\Delta\epsilon$ and of σ_{dc} at low T , the scaled frequencies $\omega\Delta\epsilon/\sigma_{dc}$ are different from that in the RSEM. Equation (2) was derived for uncorrelated barriers, but short-range correlations between neighboring barriers should not change the scaling form. This is indeed true, as evident from the inset of Fig. 5, where the data collapse at low $T \lesssim 1/40$.

However, the A-RBM shows no scaling for higher $T \gtrsim 1/40$, see in particular the data in Fig. 5 for $1/12 \leq T \leq 1/4$ corresponding to the temperature regime in Fig. 1. Hence, scaled data for the A-RBM fall onto the master curve at much lower T than in the RSEM.

This finding is relevant when interpreting experiments. For example, scaling occurs for temperatures as high as $E_{dc}/15k_B$ in sodium borate glasses [19, 20] and $E_{dc}/13k_B$ in Bi_2O_3 doped $\text{P}_2\text{O}_5\text{--V}_2\text{O}_5\text{--MoO}_3$ electronically conducting nanocomposite glass [47], corresponding to $T \cong 1/15$ and $T \cong 1/13$ in our dimensionless units ($E_{dc} \cong 1$ in

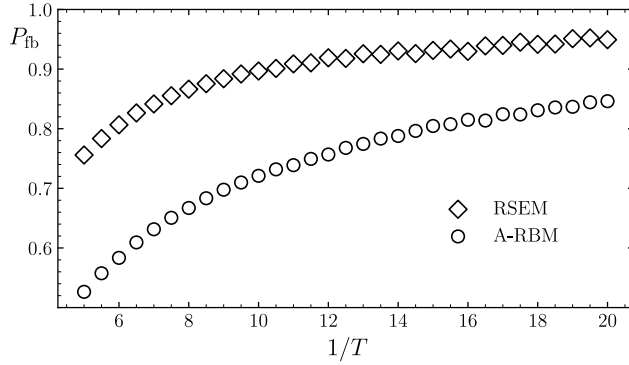


FIG. 6. Probability P_{fb} of forward-backward hopping [Eq. (9)] in equilibrium as a function of $1/T$ for the RSEM and A-RBM.

the RSEM and A-RBM). At such temperatures, a good scaling is seen in Fig. 1(b) for the RSEM but not the A-RBM in Fig. 5.

That scaling sets in at higher T in the RSEM can be understood by considering the high-frequency regime, where the scaled data of the A-RBM in Fig. 5 lie significantly below the master curve for $T \leq 1/20$ in contrast to the corresponding data of the RSEM in Fig. 2(b). At high frequencies, $\sigma(\omega)$ becomes increasingly dominated by forward-backward hopping between sites with energies slightly above and below the Fermi energy upon lowering T . The prevalence of this forward-backward hopping at a given T is more pronounced in the RSEM, where particles tend to reoccupy a site below the Fermi level after leaving it.

To corroborate this interpretation, we have analyzed forward-backward hopping probabilities P_{fb} along neighboring sites in both models. For determining P_{fb} in both the RSEM and A-RBM, we count the total number M_J of jumps and the total number M_{fb} of forward-backward jumps over a long simulation time starting from an equilibrium state. The probability then is

$$P_{\text{fb}} = \frac{M_{\text{fb}}}{M_J}. \quad (9)$$

To obtain M_{fb} , we store for each particle i in the initial equilibrium state the direction of its last jump. If particle i performs a backward jump, a counter m_i is incremented by one. If the particle i does not jump back, M_{fb} is incremented by m_i , and m_i reinitialized to zero.

Figure 6 shows P_{fb} as a function of $1/T$ for the RSEM and A-RBM. The probability of forward-backward hopping is higher for the RSEM and it increases with decreasing T towards a saturated value for both models. In the RSEM, saturation sets in for $T \lesssim 1/10$, indicating that the low- T -behavior is reached and scaled conductivity data can be expected to fall on the master curve. By contrast, P_{fb} of the A-RBM increases much slower towards the saturation limit upon lowering T . At $T = 1/20$, it is still significantly lower than in the RSEM.

V. CONCLUSIONS

In summary, we recovered the universal scaling behavior of conductivity spectra for hopping motion between sites with randomly varying energies. For the simplest case of site exclusion interaction, we demonstrated how the many-particle dynamics can be mapped onto that of independent particles hopping over barriers. The associated barrier model exhibits the same conductivity scaling as the original site energy model. However, the scaling behavior is observed at higher temperatures in the site energy model, which agrees with experimental findings [19, 20, 47].

One may wonder why the scaling should not be affected when taking into account the Coulomb interaction between the mobile charge carriers, or peculiar features present in real materials such as complex geometries of conduction paths. As for the Coulomb interaction, it is long-ranged and can be viewed to give a weakly fluctuating contribution compared to the variation of site energies, which is determined by the interaction of the mobile charge carriers with the immobile host network. Complex conduction paths arise naturally in the presence of site or barrier energy disorder due to confinement of the transport at low temperatures to percolating clusters with fractal geometry.

Our mapping of spatially fluctuating site onto barrier energies can be extended to multicomponent systems. For mixed alkali glasses with two types of mobile ions $\alpha = A, B$ having site energies E_i^α and chemical potentials μ_α , barriers for α ions are

$$U_{ij}^\alpha = \max(E_i^\alpha, E_j^\alpha) - \mu_\alpha - \sum_{k=i,j} \frac{1}{\beta} \ln [v(\beta(E_k^A - \mu_A), \beta(E_k^B - \mu_B))], \quad (10)$$

where $v(x, y) = 1/(1 + e^{-x} + e^{-y})$ for $x = \beta(E_i^A - \mu_A)$ and $y = \beta(E_i^B - \mu_B)$ is the probability that site i is vacant.

As a consequence, ions of type A and B experience distinct barrier landscapes, leading to partial conductivities $\sigma^\alpha(\omega, T)$ that scale with parameters $\sigma_{\text{dc}}^\alpha(T)$ and $\Delta\epsilon^\alpha(T)$ possessing different temperature dependencies. When the partial conductivities are similar in magnitude, the total conductivity $\sigma(\omega, T) = \sigma^A(\omega, T) + \sigma^B(\omega, T)$ is expected to show deviations from the universal time-temperature scaling, as observed in experiments [25]. We propose testing partial conductivity scaling in mixed ion conductors. The generalized mapping (10) furthermore provides a new approach for a theoretical treatment of the mixed alkali effect [106].

ACKNOWLEDGMENTS

We gratefully acknowledge financial support by the Deutsche Forschungsgemeinschaft (Project No. 428906592), and the use of a high-performance comput-

ing cluster funded by the Deutsche Forschungsgemeinschaft (Project No. 456666331).

Appendix A: KMC simulations of RSEM and calculation of frequency-dependent conductivity

For determining conductivity spectra $\sigma(\omega, T)$ of the RSEM, we have performed KMC simulations by applying the method described in Ref. [100]. In this method, the hopping of $N = nL^3 \gg 1$ particles in the presence of a sinusoidal electric field $E(t) = E_0 \sin(\omega t)$ in x -direction is considered under periodic boundary conditions in all directions. For small amplitudes E_0 with $qE_0a \ll k_B T$, the effect of the field on the hopping dynamics can be accounted for by choosing nearest-neighbor target sites for jump attempts in $\pm x$ -direction with time-dependent probabilities. In each elementary step, one of the N particles is chosen randomly and attempted to move to a nearest-neighbor site in $\pm x$ -direction with probabilities $[1 \pm qE(t)a/k_B T]/6$, and in $\pm y$ - and $\pm z$ -direction with probability 1/6. A jump attempt from site i to a vacant nearest-neighbor site j is accepted with probability $\min(1, \exp[-(E_j - E_i)/k_B T])$, and rejected if site j is occupied. After each jump attempt, time is incremented by ν/N .

Due to the applied electric field, a current in x -direction is generated that becomes stationary after a transient time. The current density in the stationary state is calculated by subdividing a period $2\pi/\omega$ of the electric field into N_{per} equidistant time intervals $[t_k - \Delta t/2, t_k + \Delta t/2]$, $k = 1, \dots, N_{\text{per}}$, where $t_k = k\Delta t - \Delta t/2$ and $\Delta t \ll 2\pi/\omega$. By counting the number N_k^+ and N_k^- of particle jumps in the $+x$ and $-x$ direction in each interval k , we obtain the current densities

$$J_k = \frac{qa}{L^3} \frac{(N_k^+ - N_k^-)}{\Delta t} \quad (\text{A1})$$

at times t_k in this period. Averaging over many periods in the stationary state gives the period-averaged current densities $\langle J_k \rangle_{\text{per}}$, and a further averaging over many realizations of the site disorder yields the period- and disorder-averaged current densities $\langle J_k \rangle_{\text{per}}$. Real and imaginary parts of the frequency-dependent conductivity are then obtained from a linear least squares fit to

$$\overline{\langle J_k \rangle}_{\text{per}} = \sigma'(\omega)E_0 \sin(\omega t_k) + \sigma''(\omega)E_0 \cos(\omega t_k). \quad (\text{A2})$$

Appendix B: Agreement of high-frequency conductivities in A-RBM and RSEM

For hopping conduction in general, σ_∞ is proportional to the mean jump rate \bar{w}_{par} of a particle in the equilibrium state [107],

$$\sigma_\infty = \frac{\beta q^2 a^2 n}{6} \bar{w}_{\text{par}}. \quad (\text{B1})$$

The rate $\bar{w}_{\text{par}}^{\text{RSEM}}$ in the equilibrium state of the RSEM is related to the mean rate $\bar{w}_{\text{Link}}^{\text{RSEM}}$ for a link to be passed by a particle by

$$\begin{aligned} \bar{w}_{\text{par}}^{\text{RSEM}} &= \frac{1}{N} \sum_i \sum_{j \text{ NN } i} \langle w_{ij} n_i \tilde{n}_j \rangle_{\text{eq}} \\ &= \frac{6M}{N} \left[\frac{1}{6M} \sum_i \sum_{j \text{ NN } i} w_{ij} \langle n_i \rangle_{\text{eq}} \langle \tilde{n}_j \rangle_{\text{eq}} \right] = \frac{6M}{N} \bar{w}_{\text{Link}}^{\text{RSEM}}, \end{aligned} \quad (\text{B2})$$

where $M = (L/a)^3$ is the number of lattice sites. and $\sum_{j \text{ NN } i} \dots$ means summation over all nearest-neighbor sites j of site i . The mean link passage rate is

$$\begin{aligned} \bar{w}_{\text{Link}}^{\text{RSEM}} &= \int dE \psi_E(E) f(\beta(E - \mu)) \\ &\quad \times \int dE' \psi_E(E') [1 - f(\beta(E' - \mu))] w(\beta(E' - E)) \end{aligned} \quad (\text{B3})$$

where $\psi_E(E)$ is the probability density of site energies E , chosen to be the Gaussian $\psi_E(E) \propto \exp(-E^2/2\Delta_E^2)$ in our modeling.

In the A-RBM with M noninteracting particles, the site occupation probabilities are $p_i = M/M = 1$ in the equilibrium state. The mean jump rate $\bar{w}_{\text{par}}^{\text{ARBM}}$ of a particle and the mean rate $\bar{w}_{\text{Link}}^{\text{ARBM}}$ for a link to be passed by a particle are related by

$$\begin{aligned} \bar{w}_{\text{par}}^{\text{ARBM}} &= \frac{1}{M} \sum_i \sum_{j \text{ NN } i} p_i \nu e^{-\beta U_{ij}} \\ &= 6 \left[\frac{1}{6M} \sum_i \sum_{j \text{ NN } i} \nu e^{-\beta U_{ij}} \right] = 6 \bar{w}_{\text{Link}}^{\text{ARBM}}. \end{aligned} \quad (\text{B4})$$

The mean link passage rate is

$$\bar{w}_{\text{Link}}^{\text{ARBM}} = \int dU \psi(U) \nu \exp(-\beta U), \quad (\text{B5})$$

where

$$\psi(U) = \int dE \int dE' \delta(U - U(E, E')) \quad (\text{B6})$$

is the probability density function of the assigned barriers. Inserting Eq. (6) into Eq. (B6), and Eq. (B6) into Eq. (B5), yields

$$\bar{w}_{\text{Link}}^{\text{ARBM}} = \bar{w}_{\text{Link}}^{\text{RSEM}}. \quad (\text{B7})$$

Using Eqs. (B2), (B4), (B7), and the number densities $n = M/Ma^3 = 1/a^3$ and $n = N/Ma^3$ for the A-RBM and RSEM, we obtain from Eq. (B1)

$$\begin{aligned} \sigma_\infty^{\text{ARBM}} &= \frac{\beta q^2 a^2}{6} \frac{1}{a^3} \bar{w}_{\text{par}}^{\text{ARBM}} = \frac{\beta q^2}{a} \bar{w}_{\text{Link}}^{\text{ARBM}} = \frac{\beta q^2}{a} \bar{w}_{\text{Link}}^{\text{RSEM}} \\ &= \frac{\beta q^2}{a} \frac{N}{6M} \bar{w}_{\text{par}}^{\text{RSEM}} = \frac{\beta q^2 a^2 n}{6} \bar{w}_{\text{par}}^{\text{RSEM}} = \sigma_\infty^{\text{RSEM}}. \end{aligned} \quad (\text{B8})$$

Hence the A-RBM with particle density $n = 1/a^3$ has the same high-frequency conductivity as the RSEM.

Appendix C: Frequency-dependent conductivity of the A-RBM calculated from velocity autocorrelation method

For calculating $\sigma(\omega, T)$ of the A-RBM we apply the velocity autocorrelation (VAC) method. This is a powerful numerical technique to calculate ac conductivities in hopping transport of noninteracting particles with symmetric jump rates [104]. We here give the relevant equations for determining $\sigma(\omega, T)$ of the A-RBM.

For our statistically isotropic system, we take the field to be in x -direction. Conductivity spectra of the A-RBM with particle number density $n = 1/a^3$ are then given by

$$\sigma(\omega) = \frac{\beta q^2 a^2}{M} i\omega \mathbf{1}_x^T \mathbf{x}(\omega), \quad (\text{C1})$$

where $\mathbf{1}_x$ and $\mathbf{x}(\omega)$ are column vectors with $3M$ elements. The first M elements of the vector $\mathbf{1}_x$ are one and the other elements are zero. The vector $\mathbf{x}(\omega)$ is determined by the inhomogeneous system of linear equations

$$(i\omega \mathbf{\Gamma}^{-1} + \mathbf{A}^T \mathbf{A}) \mathbf{x}(\omega) = \mathbf{1}_x, \quad (\text{C2})$$

where $\mathbf{\Gamma}$ is a $3M \times 3M$ block diagonal matrix

$$\mathbf{\Gamma} = \begin{pmatrix} \mathbf{\Gamma}_1 & & \\ & \mathbf{\Gamma}_2 & \\ & & \mathbf{\Gamma}_3 \end{pmatrix} \quad (\text{C3})$$

consisting of $M \times M$ matrices $\mathbf{\Gamma}_k$ in the diagonal, and \mathbf{A} is a $M \times 3M$ block row matrix $\mathbf{A} = (\mathbf{A}_1, \mathbf{A}_2, \mathbf{A}_3)$ with $M \times M$ matrices \mathbf{A}_k . The $\mathbf{\Gamma}_k$ are the $M \times M$ diagonal

matrices

$$\mathbf{\Gamma}_k = \begin{pmatrix} \Gamma_{i(1)}^{k+} & \cdots & 0 \\ \ddots & \ddots & \\ 0 & \cdots & \Gamma_{i(M)}^{k+} \end{pmatrix}. \quad (\text{C4})$$

with $\Gamma_{i(j)}^{k+} = \nu \exp[-\beta U_{i(j)}^{k+}]$ the jump rate from site $i(j)$ in positive k direction and $U_{i(j)}$ the barrier to be surmounted for a corresponding jump. The multindex $i(j) = (i_1(j), i_2(j), i_3(j))$ gives the position of a site in the three-dimensional array and j indices the same site after a vectorization of the array with i_1 the fastest running index, i.e.

$$j = i_1 + (i_2 - 1)M_0 + (i_3 - 1)M_0^2, \quad (\text{C5})$$

$i_k = 1, \dots, M_0$, where $M_0 = L/a = M^{1/3}$ is the number of lattice sites in along one coordinate axis.

The \mathbf{A}_k are representing matrices for a discrete derivative in k th direction under periodic boundary conditions. Specifically,

$$\mathbf{A}_1 = \mathbf{I} \otimes \mathbf{I} \otimes \mathbf{A}_0, \quad \mathbf{A}_2 = \mathbf{I} \otimes \mathbf{A}_0 \otimes \mathbf{I}, \quad \mathbf{A}_3 = \mathbf{A}_0 \otimes \mathbf{I} \otimes \mathbf{I}, \quad (\text{C6})$$

where \otimes denotes the Kronecker product operation, \mathbf{I} is the $M_0 \times M_0$ identity matrix, and \mathbf{A}_0 is the $M_0 \times M_0$ matrix

$$\mathbf{A}_0 = \begin{pmatrix} 1 & 0 & 0 & 0 & \cdots & 0 & -1 \\ -1 & 1 & 0 & 0 & \cdots & 0 & 0 \\ 0 & -1 & 1 & 0 & \cdots & 0 & 0 \\ & & & & \ddots & & \\ 0 & 0 & 0 & 0 & \cdots & -1 & 1 \end{pmatrix}. \quad (\text{C7})$$

Equation (C2) can be solved numerically with high computational efficiency by linear equation solvers even for large $\beta = 1/k_B T$.

[1] S. Summerfield, Universal low-frequency behaviour in the a.c. hopping conductivity of disordered systems, *Philos. Mag. B* **52**, 9 (1985).

[2] J. C. Dyre and T. B. Schröder, Universality of ac conduction in disordered solids, *Rev. Mod. Phys.* **72**, 873 (2000).

[3] S. Abboudy, P. Fozooni, R. Mansfield, and M. J. Lea, Finite frequency scaling of hopping conductivity in n-InSb, *Phil. Mag. Lett.* **57**, 277 (1988).

[4] M. Ben-Chorin, F. Möller, F. Koch, W. Schirmacher, and M. Eberhard, Hopping transport on a fractal: ac conductivity of porous silicon, *Phys. Rev. B* **51**, 2199 (1995).

[5] C. Çil and G. Aktas, Frequency-dependent conductivity in evaporated amorphous silicon films, *Thin Solid Films* **196**, 179 (1991).

[6] C. Godet, J. Kleider, and A. Gudovskikh, Frequency scaling of ac hopping transport in amorphous carbon nitride, *Diamond Relat. Mater.* **16**, 1799 (2007), proceedings of the 6th Specialists Meeting in Amorphous Carbon.

[7] W. Rehwald, H. Kiess, and B. Binggeli, Frequency dependent conductivity in polymers and other disordered materials, *Z. Phys. B* **68**, 143 (1987).

[8] M. M. Jastrzebska, S. Jussila, and H. Isotalo, Dielectric response and a.c. conductivity of synthetic dopa-melanin polymer, *J. Mater. Sci.* **33**, 4023 (1998).

[9] H. B. Brom, J. A. Reedijk, H. C. F. Martens, L. J. Adriaanse, L. J. de Jongh, M. A. J. Michels, and M. A. J. Michels, Frequency and temperature scaling in the conductivity and its structural consequences, *phys. stat. sol. b* **205**, 103 (1998).

[10] I. Garoui, S. Hajlaoui, M. Tliha, R. Naouari, S. Nasri, A. Ouasri, J. Lhoste, and A. Oueslati, New organic-inorganic chloride (2-amino-4-methylpyridinium hexachlorostannate): Crystal structure, BFDH morphol-

ogy, and electrical conduction mechanism, *J. Phys. Chem. Solids* **206**, 112840 (2025).

[11] B. E. Kilbride, J. N. Coleman, J. Fraysse, P. Fournet, M. Cadek, A. Drury, S. Hutzler, S. Roth, and W. J. Blau, Experimental observation of scaling laws for alternating current and direct current conductivity in polymer-carbon nanotube composite thin films, *J. Appl. Phys.* **92**, 4024 (2002).

[12] L. Zuppiroli, N. Papandreu, and R. Kormann, The dielectric response of boron carbide due to hopping conduction, *J. Appl. Phys.* **70**, 246 (1991).

[13] Y. Nagao, I. Terasaki, and T. Nakano, Dielectric constant and ac conductivity of the layered cobalt oxide $\text{Bi}_2\text{Sr}_2\text{CoO}_{6+\delta}$: A possible metal-dielectric composite made by self-organization of Co^{2+} and Co^{3+} ions, *Phys. Rev. B* **76**, 144203 (2007).

[14] A. Ghodhbani, Y. Moualhi, W. Dimassi, R. M'nassri, H. Rahmouni, and K. Khirouni, Contribution of strong electron-phonon interaction in the transport properties of $\text{La}_{0.8}\text{Ca}_{0.2}\text{Mn}_{0.5}\text{Ni}_{0.5}\text{O}_3$ system, *Phys. B Condens. Matter* **683**, 415964 (2024).

[15] S. A. Rozanski, F. Kremer, P. Köberle, and A. Laschewsky, Relaxation and charge transport in mixtures of zwitterionic polymers and inorganic salts, *Macromol. Chem. Phys.* **196**, 877 (1995).

[16] A. Khiar, R. Puteh, and A. Arof, Conductivity studies of a chitosan-based polymer electrolyte, *Physica B* **373**, 23 (2006).

[17] A. W. Imre, M. Schönhoff, and C. Cramer, Unconventional scaling of electrical conductivity spectra for PSS-PDADMAC polyelectrolyte complexes, *Phys. Rev. Lett.* **102**, 255901 (2009).

[18] P. Pal and A. Ghosh, Dynamics and relaxation of charge carriers in poly(methylmethacrylate)-based polymer electrolytes embedded with ionic liquid, *Phys. Rev. E* **92**, 062603 (2015).

[19] B. Roling, A. Happe, K. Funke, and M. D. Ingram, Carrier concentrations and relaxation spectroscopy: New information from scaling properties of conductivity spectra in ionically conducting glasses, *Phys. Rev. Lett.* **78**, 2160 (1997).

[20] B. Roling, Scaling properties of the conductivity spectra of glasses and supercooled melts, *Solid State Ionics* **105**, 185 (1998).

[21] A. Pan and A. Ghosh, Activation energy and conductivity relaxation of sodium tellurite glasses, *Phys. Rev. B* **59**, 899 (1999).

[22] B. Roling, C. Martiny, and K. Funke, Information on the absolute length scales of ion transport processes in glasses from electrical conductivity and tracer diffusion data, *J. Non-Cryst. Solids* **249**, 201 (1999).

[23] R. Belin, G. Taillades, A. Pradel, and M. Ribes, Ion dynamics in superionic chalcogenide glasses: Complete conductivity spectra, *Solid State Ionics* **136-137**, 1025 (2000).

[24] A. Ghosh and A. Pan, Scaling of the conductivity spectra in ionic glasses: Dependence on the structure, *Phys. Rev. Lett.* **84**, 2188 (2000).

[25] C. Cramer, S. Brückner, Y. Gao, and K. Funke, Ion dynamics in mixed alkali glasses, *Phys. Chem. Chem. Phys.* **4**, 3214 (2002).

[26] C. Cramer, S. Brunklaus, Y. Gao, and K. Funke, Dynamics of mobile ions in single- and mixed-cation glasses, *J. Phys. Condens. Matter* **15**, S2309 (2003).

[27] D. Dutta and A. Ghosh, Dynamics of Ag^+ ions in binary tellurite glasses, *Phys. Rev. B* **72**, 024201 (2005).

[28] S. Bhattacharya and A. Ghosh, Relaxation dynamics in superionic glass nanocomposites, *J. Am. Ceram. Soc.* **91**, 753 (2007).

[29] H. Staesche and B. Roling, Nonlinear conductivity spectra of ionically conducting glasses and glass ceramics: Analysis of spectral shape and scaling properties, *Phys. Rev. B* **82**, 134202 (2010).

[30] A. A. Ali and M. H. Shaaban, Electrical properties and scaling behaviour of Sm^{3+} doped CaF_2 -bismuth borate glasses, *Bull. Mater. Sci.* **34**, 491 (2011).

[31] B. Deb and A. Ghosh, Silver ion dynamics in Ag_2S -doped silver molybdate-glass nanocomposites: Correlation of conductivity and scaling with structure, *J. Phys. Chem. C* **115**, 14141 (2011).

[32] J. R. Sangoro and F. Kremer, Charge transport and glassy dynamics in ionic liquids, *Acc. Chem. Res.* **45**, 525 (2012).

[33] P. Singh, B. P. Singh, and Raghvendra, Dispersion in AC conductivity of fragile glass melts near glass transition temperature, *Solid State Ionics* **227**, 39 (2012).

[34] M. Purnima, S. Bale, M. Samee, S. K. Ahmmad, and S. Rahman, AC conductivity and its scaling behavior in $\text{MgO}-\text{Li}_2\text{O}-\text{B}_2\text{O}_3-\text{Bi}_2\text{O}_3$ glasses, *J. Phys. Chem. Solids* **74**, 189 (2013).

[35] R. Christensen, G. Olson, and S. W. Martin, Ionic conductivity of mixed glass former $0.35\text{Na}_2\text{O}+0.65[x\text{B}_2\text{O}_3+(1-x)\text{P}_2\text{O}_5]$ glasses, *J. Phys. Chem. B* **117**, 16577 (2013).

[36] K. Sklepić, M. Vorokhta, P. Mošner, L. Koudelka, and A. Moguš-Milanković, Electrical mobility of silver ion in $\text{Ag}_2\text{O}-\text{B}_2\text{O}_3-\text{P}_2\text{O}_5-\text{TeO}_2$ glasses, *J. Phys. Chem. B* **118**, 12050 (2014), PMID: 25242657.

[37] S. K. Chaurasia, A. L. Saroj, Shalu, V. K. Singh, A. K. Tripathi, A. K. Gupta, Y. L. Verma, and R. K. Singh, Studies on structural, thermal and AC conductivity scaling of PEO-LiPF₆ polymer electrolyte with added ionic liquid [BMIMPF₆], *AIP Adv.* **5**, 077178 (2015).

[38] S. N. Tripathy, Z. Wojnarowska, J. Knapik, H. Shirota, R. Biswas, and M. Paluch, Glass transition dynamics and conductivity scaling in ionic deep eutectic solvents: The case of (acetamide + lithium nitrate/sodium thiocyanate) melts, *J. Chem. Phys.* **142**, 184504 (2015).

[39] S. Nasri, M. Megdiche, and M. Gargouri, DC conductivity and study of AC electrical conduction mechanisms by non-overlapping small polaron tunneling model in LiFeP_2O_7 ceramic, *Ceram. Int.* **42**, 943 (2016).

[40] D. Singh, K. Shahi, and K. K. Kar, Superlinear frequency dependence of AC conductivity and its scaling behavior in $x\text{AgI}-(1-x)\text{AgPO}_3$ glass superionic conductors, *Solid State Ionics* **287**, 89 (2016).

[41] S. S. Gandi, S. Gandi, N. K. Katari, D. P. Dutta, and B. R. Ravuri, Electrical properties and scaling studies of $\text{Na}_{3+x}\text{Zr}_x\text{Sc}_{2-x}(\text{PO}_4)_3$ glass ceramic electrolyte for use in Na-ion batteries, *Appl. Phys. A* **125**, 92 (2019).

[42] A. Palui and A. Ghosh, Structure-transport correlation of super-ionic mixed network former glasses, *Solid State Ionics* **343**, 115126 (2019).

[43] K. H. Sadok, M. Haouari, O. Gallot-Lavallée, and H. Ben Ouada, Effect of Na_2SO_4 substitution for Na_2O on the structural and electrical properties of a sodium borophosphate glass, *J. Alloys Compd.* **778**, 878 (2019).

[44] S. Ojha, M. S. Ali, M. Roy, and S. Bhattacharya, Hop-

ping frequency and conductivity relaxation of promising chalcogenides: AC conductivity and dielectric relaxation approaches, *Mater. Res. Express* **8**, 085203 (2021).

[45] J. Ghosh, A. Sengupta, P. Halder, S. Ojha, G. K. Panda, and S. Bhattacharya, Single polaron hopping in Fe doped glassy semiconductors: Structure–electrical transport relationship, *J. Appl. Phys.* **132**, 205108 (2022).

[46] N. H. Makani, A. Sahoo, P. Pal, T. Paul, L. S. Tanwar, M. Singh, A. Ghosh, and R. Banerjee, Onset of vacancy-mediated high activation energy leads to large ionic conductivity in two-dimensional layered $\text{Cs}_2\text{PbI}_2\text{Cl}_2$ Ruddlesden-Popper halide perovskite, *Phys. Rev. Mater.* **6**, 115002 (2022).

[47] A. Mandal, N. Modak, A. Rakshit, R. Mondal, A. S. Das, S. Kabi, S. Mondal, and D. Biswas, Structural modifications, optical response, and electrical conductivity mechanism of Bi_2O_3 doped in $\text{P}_2\text{O}_5\text{-V}_2\text{O}_5\text{-MoO}_3$ nanocomposite glass systems, *Mater. Chem. Phys.* **298**, 127466 (2023).

[48] S. Summerfield and P. N. Butcher, A unified equivalent-circuit approach to the theory of ac and dc hopping conductivity in disordered systems, *J. Phys. C: Solid State Phys.* **15**, 7003 (1982).

[49] A. Hunt, Transport in ionic conducting glasses. II. Scaling relations and approximate power law behaviour, *J. Phys.: Condens. Matter* **4**, 5371 (1992).

[50] A. Hunt, The low frequency conductivity of the Fermi glass, *J. Phys.: Condens. Matter* **4**, 6957 (1992).

[51] S. D. Baranovskii and H. Cordes, On the conduction mechanism in ionic glasses, *J. Chem. Phys.* **111**, 7546 (1999).

[52] J. C. Dyre, The random free-energy barrier model for ac conduction in disordered solids, *J. Appl. Phys.* **64**, 2456 (1988).

[53] J. C. Dyre and J. M. Jacobsen, Universal time dependence of the mean-square displacement in extremely rugged energy landscapes with equal minima, *Phys. Rev. E* **52**, 2429 (1995).

[54] J. C. Dyre and T. B. Schröder, Effective one-dimensionality of universal ac hopping conduction in the extreme disorder limit, *Phys. Rev. B* **54**, 14884 (1996).

[55] B. Roling, Modeling of ion transport processes in disordered solids: Monte Carlo simulations of the low-temperature particle dynamics in the random barrier model, *Phys. Chem. Chem. Phys.* **3**, 5093 (2001).

[56] J. C. Dyre and T. B. Schröder, Hopping models and ac universality, *physica status solidi (b)* **230**, 5 (2002).

[57] T. B. Schröder and J. C. Dyre, Computer simulations of the random barrier model, *Phys. Chem. Chem. Phys.* **4**, 3173 (2002).

[58] T. B. Schröder and J. C. Dyre, ac Hopping conduction at extreme disorder takes place on the percolating cluster, *Phys. Rev. Lett.* **101**, 025901 (2008).

[59] T. B. Schröder and J. C. Dyre, Scaling and universality of ac conduction in disordered solids, *Phys. Rev. Lett.* **84**, 310 (2000).

[60] D. E. Day, Mixed alkali glasses — their properties and uses, *J. Non-Cryst. Solids* **21**, 343 (1976).

[61] P. Maass, A. Bunde, and M. D. Ingram, Ion transport anomalies in glasses, *Phys. Rev. Lett.* **68**, 3064 (1992).

[62] S. Balasubramanian and K. J. Rao, Preferential paths in alkali ion migration and the mixed alkali effect in silicate glasses, *J. Phys. Chem.* **97**, 8835 (1993).

[63] J. Habasaki, I. Okada, and Y. Hiwatari, Md study of the mixed alkali effect in a lithium-potassium metasilicate glass, *J. Non-Cryst. Solids* **183**, 12 (1995).

[64] P. Maass, Towards a theory for the mixed alkali effect in glasses, *J. Non-Cryst. Solids* **255**, 35 (1999).

[65] A. G. Hunt, Mixed-alkali effect: some new results, *J. Non-Cryst. Solids* **255**, 47 (1999).

[66] R. Kirchheim, The mixed alkali effect as a consequence of network density and site energy distribution, *J. Non-Cryst. Solids* **272**, 85 (2000).

[67] J. Swenson, A. Matic, C. Karlsson, L. Börjesson, C. Meneghini, and W. S. Howells, Random ion distribution model: A structural approach to the mixed-alkali effect in glasses, *Phys. Rev. B* **63**, 132202 (2001).

[68] M. D. Ingram and B. Roling, The concept of matrix-mediated coupling: a new interpretation of mixed-cation effects in glass, *J. Phys.: Condens. Matter* **15**, S1595 (2003).

[69] J. Swenson and S. Adams, Mixed alkali effect in glasses, *Phys. Rev. Lett.* **90**, 155507 (2003).

[70] J. Habasaki, K. L. Ngai, and Y. Hiwatari, “Cooperativity blockage” in the mixed alkali effect as revealed by molecular-dynamics simulations of alkali metasilicate glass, *J. Chem. Phys.* **121**, 925 (2004).

[71] H. Lammert and A. Heuer, Contributions to the mixed-alkali effect in molecular dynamics simulations of alkali silicate glasses, *Phys. Rev. B* **72**, 214202 (2005).

[72] R. Peibst, S. Schott, and P. Maass, Internal friction and vulnerability of mixed alkali glasses, *Phys. Rev. Lett.* **95**, 115901 (2005).

[73] P. Maass and R. Peibst, Ion diffusion and mechanical losses in mixed alkali glasses, *J. Non-Cryst. Solids* **352**, 5178 (2006).

[74] G. K. Kumari, S. M. Begum, C. R. Krishna, D. Sathish, P. Murthy, P. Rao, and R. Ravikumar, Physical and optical properties of Co^{2+} , Ni^{2+} doped $20\text{ZnO}+x\text{Li}_2\text{O}+(30-x)\text{K}_2\text{O}+50\text{B}_2\text{O}_3$ ($5 \leq x \leq 25$) glasses: Observation of mixed alkali effect, *Mater. Res. Bull.* **47**, 2646 (2012).

[75] J. E. Tsuchida, F. A. Ferri, P. S. Pizani, A. C. Martins Rodrigues, S. Kundu, J. F. Schneider, and E. D. Zanotto, Ionic conductivity and mixed-ion effect in mixed alkali metaphosphate glasses, *Phys. Chem. Chem. Phys.* **19**, 6594 (2017).

[76] Z. Shan, S. Liu, H. Tao, and Y. Yue, Mixed alkaline-earth effects on several mechanical and thermophysical properties of aluminate glasses and melts, *J. Am. Ceram. Soc.* **102**, 1128 (2019).

[77] C. J. Wilkinson, A. R. Potter, R. S. Welch, C. Bragatto, Q. Zheng, M. Bauchy, M. Affatigato, S. A. Feller, and J. C. Mauro, Topological origins of the mixed alkali effect in glass, *J. Phys. Chem. B* **123**, 7482 (2019).

[78] F. Noritake and S. Naito, Mechanism of mixed alkali effect in silicate glass/liquid: Pathway and network analysis, *J. Non-Cryst. Solids* **610**, 122321 (2023).

[79] V. K. Deshpande, A. Pradel, and M. Ribes, The mixed glass former effect in the $\text{Li}_2\text{S} : \text{SiS}_2 : \text{GeS}_2$ system, *Mater. Res. Bull.* **23**, 379 (1988).

[80] G. Jayasinghe, P. Bandaranayake, and J. Souquet, Mixed former effect in sodium phospho tellurate glasses, *Solid State Ionics* **86-88**, 447 (1996).

[81] A. Pradel, N. Kuwata, and M. Ribes, Ion transport and structure in chalcogenide glasses, *J. Phys. Condens. Matter* **15**, S1561 (2003).

[82] P. S. Anantha and K. Hariharan, Structure and ionic transport studies of sodium borophosphate glassy system, *Mater. Chem. Phys.* **89**, 428 (2005).

[83] D. Zielniok, C. Cramer, and H. Eckert, Structure property correlations in ion-conducting mixed-network former glasses: Solid-state NMR studies of the system $\text{Na}_2\text{O}\text{-B}_2\text{O}_3\text{-P}_2\text{O}_5$, *Chem. Mat.* **19**, 3162 (2007).

[84] D. Raskar, M. T. Rinke, and H. Eckert, The mixed-network former effect in phosphate glasses: NMR and XPS studies of the connectivity distribution in the glass system $(\text{NaPO}_3)_{1-x}(\text{B}_2\text{O}_3)x$, *J. Phys. Chem. C* **112**, 12530 (2008).

[85] M. J. Haynes, C. Bischoff, T. Kaufmann, and S. W. Martin, The mixed glass former effect on the thermal and volume properties of $\text{Na}_2\text{S}\text{-B}_2\text{S}_3\text{-P}_2\text{S}_5$ glasses, *Phys. Chem. Glasses: Eur. J. of Glass Science and Technol. Part B* **50**, 144 (2009).

[86] M. Schuch, C. R. Müller, P. Maass, and S. W. Martin, Mixed barrier model for the mixed glass former effect in ion conducting glasses, *Phys. Rev. Lett.* **102**, 145902 (2009).

[87] M. Schuch, C. Trott, and P. Maass, Network forming units in alkali borate and borophosphate glasses and the mixed glass former effect, *RSC Adv.* **1**, 1370 (2011).

[88] D. Larink, H. Eckert, M. Reichert, and S. W. Martin, Mixed network former effect in ion-conducting alkali borophosphate glasses: Structure/property correlations in the system $[\text{M}_2\text{O}]_{1/3}[(\text{B}_2\text{O}_3)_x(\text{P}_2\text{O}_5)_{1-x}]_{2/3}$ ($\text{M}=\text{Li}, \text{K}, \text{Cs}$), *J. Phys. Chem. C* **116**, 26162 (2012).

[89] A. Shaw and A. Ghosh, Dynamics of lithium ions in borotellurite mixed former glasses: Correlation between the characteristic length scales of mobile ions and glass network structural units, *J. Chem. Phys.* **141**, 164504 (2014).

[90] M. Karlsson, M. Schuch, R. Christensen, P. Maass, S. W. Martin, S. Imberti, and A. Matic, Structural origin of the mixed glass former effect in sodium borophosphate glasses investigated with neutron diffraction and reverse Monte Carlo modeling, *J. Phys. Chem. B* **119**, 27275 (2015).

[91] D. Larink, M. T. Rinke, and H. Eckert, Mixed network former effects in tellurite glass systems: Structure/property correlations in the system $(\text{Na}_2\text{O})_{1/3}[(2\text{TeO}_2)_x(\text{P}_2\text{O}_5)_{1-x}]_{2/3}$, *J. Phys. Chem. C* **119**, 17539 (2015).

[92] S. W. Martin, C. Bischoff, and K. Schuller, Composition dependence of the Na^+ ion conductivity in $0.5\text{Na}_2\text{S}+0.5x\text{GeS}_2+(1-x)\text{PS}_{5/2}$ mixed glass former glasses: A structural interpretation of a negative mixed glass former effect, *J. Phys. Chem. B* **119**, 15738 (2015).

[93] S. W. Martin, R. Christensen, G. Olson, J. Kieffer, and W. Wang, New interpretation of Na^+ -ion conduction in and the structures and properties of sodium borosilicate mixed glass former glasses, *J. Phys. Chem. C* **123**, 5853 (2019).

[94] W. F. Pasveer, P. A. Bobbert, and M. A. J. Michels, Universality of AC conductivity: Random site-energy model with Fermi statistics, *Phys. Rev. B* **74**, 165209 (2006).

[95] M. Porto, P. Maass, M. Meyer, A. Bunde, and W. Dieterich, Hopping transport in the presence of site-energy disorder: Temperature and concentration scaling of conductivity spectra, *Phys. Rev. B* **61**, 6057 (2000).

[96] J. W. Haus and K. W. Kehr, Diffusion in regular and disordered lattices, *Phys. Rep.* **150**, 263 (1987).

[97] H. Lammert, M. Kunow, and A. Heuer, Complete identification of alkali sites in ion conducting lithium silicate glasses: A computer study of ion dynamics, *Phys. Rev. Lett.* **90**, 215901 (2003).

[98] J. Habasaki and Y. Hiwatari, Molecular dynamics study of the mechanism of ion transport in lithium silicate glasses: Characteristics of the potential energy surface and structures, *Phys. Rev. B* **69**, 144207 (2004).

[99] C. Müller, E. Zienicke, S. Adams, J. Habasaki, and P. Maass, Comparison of ion sites and diffusion paths in glasses obtained by molecular dynamics simulations and bond valence analysis, *Phys. Rev. B* **75**, 014203 (2007).

[100] P. Maass, M. Meyer, and A. Bunde, Nonstandard relaxation behavior in ionically conducting materials, *Phys. Rev. B* **51**, 8164 (1995).

[101] Higher frequencies reflect short-time dynamics, where for modeling measured spectra one needs to take account the dynamics of the charge carriers in their potential wells, which is not covered by the hopping model.

[102] V. Ambegaokar, B. I. Halperin, and J. S. Langer, Hopping conductivity in disordered systems, *Phys. Rev. B* **4**, 2612 (1971).

[103] A. Miller and E. Abrahams, Impurity conduction at low concentrations, *Phys. Rev.* **120**, 745 (1960).

[104] T. B. Schröder, *Hopping in Disordered Media: A Model Glass Former and a Hopping Model*, Ph.D. thesis, Roskilde Universitet, Denmark (2000), arXiv:cond-mat/0005127.

[105] J. Hoshen and R. Kopelman, Percolation and cluster distribution. I. Cluster multiple labeling technique and critical concentration algorithm, *Phys. Rev. B* **14**, 3438 (1976).

[106] J. Leiber, *Fermi lattice gas model for mixed alkali effect in ion conducting glasses*, Master's thesis, School of Physics, Osnabrück University (2025).

[107] W. Dieterich, P. Fulde, and I. Peschel, Theoretical models for superionic conductors, *Adv. Phys.* **29**, 527 (1980).